BRAIN
A JOURNAL OF NEUROLOGY

GWAS of longitudinal amyloid accumulation on ^{18}F-florbetapir PET in Alzheimer's disease implicates microglial activation gene *IL1RAP*

Vijay K. Ramanan,[1,2,3,4] Shannon L. Risacher,[1,4] Kwangsik Nho,[1,4,5] Sungeun Kim,[1,4,5] Li Shen,[1,4,5] Brenna C. McDonald,[1,4,6] Karmen K. Yoder,[1] Gary D. Hutchins,[1] John D. West,[1] Eileen F. Tallman,[1] Sujuan Gao,[4,7] Tatiana M. Foroud,[1,2,4,5] Martin R. Farlow,[4,6] Philip L. De Jager,[8,9,10] David A. Bennett,[11] Paul S. Aisen,[12] Ronald C. Petersen,[13] Clifford R. Jack, Jr.,[14] Arthur W. Toga,[15] Robert C. Green,[16] William J. Jagust,[17] Michael W. Weiner,[18,19] and Andrew J. Saykin,[1,2,4,5] for the Alzheimer's Disease Neuroimaging Initiative (ADNI)*

Brain amyloid deposition is thought to be a seminal event in Alzheimer's disease. To identify genes influencing Alzheimer's disease pathogenesis, we performed a genome-wide association study of longitudinal change in brain amyloid burden measured by ^{18}F-florbetapir PET. A novel association with higher rates of amyloid accumulation independent from *APOE* (apolipoprotein E) $\varepsilon 4$ status was identified in *IL1RAP* (interleukin-1 receptor accessory protein; rs12053868-G; $P = 1.38 \times 10^{-9}$) and was validated by deep sequencing. *IL1RAP* rs12053868-G carriers were more likely to progress from mild cognitive impairment to Alzheimer's disease and exhibited greater longitudinal temporal cortex atrophy on MRI. In independent cohorts rs12053868-G was associated with accelerated cognitive decline and lower cortical ^{11}C-PBR28 PET signal, a marker of microglial activation. These results suggest a crucial role of activated microglia in limiting amyloid accumulation and nominate the IL-1/IL1RAP pathway as a potential target for modulating this process.

1   Centre for Neuroimaging, Department of Radiology and Imaging Sciences, Indiana University School of Medicine, Indianapolis, IN 46202, USA
2   Department of Medical and Molecular Genetics, Indiana University School of Medicine, Indianapolis, IN 46202, USA
3   Medical Scientist Training Program, Indiana University School of Medicine, Indianapolis, IN 46202, USA
4   Indiana Alzheimer Disease Centre, Indiana University School of Medicine, Indianapolis, IN 46202, USA
5   Centre for Computational Biology and Bioinformatics, Indiana University School of Medicine, Indianapolis, IN 46202, USA
6   Department of Neurology, Indiana University School of Medicine, Indianapolis, IN 46202, USA
7   Department of Biostatistics, Indiana University School of Medicine, Indianapolis, IN 46202, USA
8   Program in Translational NeuroPsychiatric Genomics, Institute for the Neurosciences, Brigham and Women's Hospital, Boston, MA 02115, USA
9   Departments of Neurology and Psychiatry, Harvard Medical School, Boston, MA 02115, USA
10 Program in Medical and Population Genetics, Broad Institute, Cambridge, MA 02142, USA
11 Rush Alzheimer's Disease Centre, Rush University Medical Centre, Chicago, IL 60612, USA

12 University of Southern California Alzheimer's Therapeutic Research Institute, San Diego, CA 92121, USA
13 Department of Neurology, Mayo Clinic Minnesota, Rochester, MN 55905, USA
14 Department of Radiology, Mayo Clinic Minnesota, Rochester, MN 55905, USA
15 Laboratory of NeuroImaging, Keck School of Medicine, University of Southern California, Los Angeles, CA 90033, USA
16 Division of Genetics, Department of Medicine, Brigham and Women's Hospital and Harvard Medical School, Boston, MA 02115, USA
17 Department of Neurology, University of California, Berkeley, CA 94720, USA
18 Departments of Radiology, Medicine, and Psychiatry, University of California-San Francisco, San Francisco, CA 94143, USA
19 Department of Veterans Affairs Medical Centre, San Francisco, CA 94121, USA

Correspondence to: Andrew J. Saykin,
IU Health Neuroscience Centre,
355 West 16th Street,
Suite 4100, Indianapolis,
IN 46202, USA
E-mail: asaykin@iupui.edu

Introduction

Deposition of amyloid-β in the brain is thought to be a necessary early step in the development of Alzheimer's disease, a progressive and highly prevalent neurodegenerative disorder with substantial societal burdens (Karran *et al.*, 2011; Jack *et al.*, 2013*a*). Existing prospective studies suggest that brain amyloid accumulation occurs over decades, preceding the onset of clinical symptoms and subsequently contributing to clinical progression (Villemagne *et al.*, 2013; Doraiswamy *et al.*, 2014; Huijbers *et al.*, 2015). However, the mechanisms underlying amyloid accumulation and clearance in Alzheimer's disease are not fully understood.

Pathogenic mutations causing rare, early-onset forms of Alzheimer's disease have been described in three genes involved in amyloidogenesis, *APP* (amyloid precursor protein), *PSEN1* (presenilin 1), and *PSEN2* (presenilin 2) (Bettens *et al.*, 2013). For late-onset Alzheimer's disease, the strongest known genetic risk factor is the *APOE* ε4 allele (Corder *et al.*, 1993). Several mechanisms have been proposed relating *APOE* ε4 to enhanced aggregation and reduced clearance of brain amyloid (Kim *et al.*, 2009). However, *APOE* ε4 is neither necessary nor sufficient for development of amyloid pathology or incident Alzheimer's disease, suggesting that other contributing factors remain to be discovered.

With the development of radiotracers allowing for non-invasive *in vivo* detection of amyloid plaque burden in large samples (Clark *et al.*, 2012), amyloid PET has become an established endophenotype used in cross-sectional studies to relate genetic variants to Alzheimer's disease pathology (Swaminathan *et al.*, 2012; Rhinn *et al.*, 2013; Shulman *et al.*, 2013; Lim *et al.*, 2014; Ramanan *et al.*, 2014*b*). We hypothesized that genetic factors would also modulate the rate of amyloid accumulation over time. We therefore performed a genome-wide association study (GWAS) of longitudinal change in brain amyloid burden measured by ^{18}F-florbetapir PET to identify novel genetic influences on the pathogenesis and trajectory of Alzheimer's disease.

Materials and methods

Subjects and phenotypes

The Alzheimer's Disease Neuroimaging Initiative (ADNI, Weiner *et al.*, 2010), Indiana Memory and Aging Study (IMAS; Ramanan *et al.*, 2014*a*), Rush Memory and Aging Project (MAP, Bennett *et al.*, 2012*b*), and Religious Orders Study (ROS; Bennett *et al.*, 2012*a*) are longitudinal studies of older adults representing clinical stages along the continuum from normal ageing to Alzheimer's disease. All participants provided written informed consent, and study protocols were approved by each site's institutional review board.

[18]F-Florbetapir PET imaging was performed at baseline and 2-year follow-up for participants enrolled in the ADNI GO and 2 phases. Image acquisition and preprocessing were performed as described previously (Jagust *et al.*, 2010). Tracer uptake was normalized to average uptake values from an atlas-based composite reference region expected not to exhibit amyloid pathology (composed of the cerebral white matter degraded to 0.7, brainstem, and whole cerebellum). This normalization yielded standardized uptake value ratio (SUVR) images (Schmidt *et al.*, 2014). As described previously, the mean SUVR for a customized composite region was obtained to represent a global cortical measure of amyloid burden at each time point (Risacher *et al.*, 2015). The annualized per cent change in global cortical SUVR at 2-year follow-up compared to baseline was used as the main quantitative phenotype for genetic analysis. Extreme outliers (annualized per cent change > three standard deviations from the sample mean) were excluded to limit the potential for spurious associations.

For *post hoc* analyses, baseline amyloid status (positive versus negative) was determined for each participant as described previously (Risacher *et al.*, 2015).

[11]C-PBR28 PET imaging was performed for a subset of IMAS participants as described previously (Yoder *et al.*, 2013). The sample analysed included cognitively normal older adults (*n* = 7), older adults with cognitive complaints in the absence of significant cognitive deficits (*n* = 5), participants with mild cognitive impairment (MCI, *n* = 7), and clinical Alzheimer's disease participants (*n* = 6). SUV images were created by normalizing each voxel by the injected dose of ^{11}C-PBR28 per total body weight. Mean SUV data were extracted for the frontal, parietal, temporal, limbic, and occipital lobes. The average SUV for these five regions was calculated to represent a global cortical index of activated microglia for use as a quantitative phenotype. *TSPO* (translocator protein, 18 kDa) rs6971 genotype was used to delineate participants with high, mixed, and low affinity states of the TSPO binding site, as ^{11}C-PBR28 is highly sensitive to these states (Kreisl *et al.*, 2013). For genetic analyses, participants with low affinity TSPO binding sites (rs6971-TT) were excluded and rs6971 genotype (CC versus TC) was included as a covariate (Yoder *et al.*, 2013).

For ADNI participants, structural MRI scans from baseline and 2-year follow-up visits were downloaded (www.adni.loni.usc.edu) and processed as described previously (Risacher *et al.*, 2010) using FreeSurfer, version 5.1. For each scan, mean thickness values from the left and right temporal cortex regions were averaged to create a measure of bilateral temporal cortex thickness. The annualized per cent change in bilateral temporal cortex thickness at 2-year follow-up compared to baseline was calculated for use in genetic analyses.

Verbal episodic memory performance was assessed at baseline and 2-year follow-up for participants from ADNI, MAP and ROS using delayed recall of logical memory prose passages from the Wechsler Memory Scale-Revised. For genetic analyses, the 2-year difference in delayed recall score was used as the phenotype and baseline age, gender and education were included as covariates.

Genotyping and imputation

GWAS data for ADNI participants were obtained and processed as described previously (Ramanan *et al.*, 2014b). Briefly, genotyping was performed per manufacturer's protocol using blood genomic DNA samples and Illumina GWAS arrays (610-Quad, OmniExpress, or HumanOmni2.5-4v1). The single nucleotide polymorphisms (SNPs) characterizing *APOE ε2/ε3/ε4* status (rs429358 and rs7412) were genotyped separately and merged with the array data sets as described previously (Saykin *et al.*, 2010, 2015). Genotype data underwent stringent quality control including identity checks, sample exclusion for call rate <95%, and SNP exclusion for call rate <95%, Hardy-Weinberg $P < 1 \times 10^{-6}$, or minor allele frequency (MAF) <1%.

MaCH (Li *et al.*, 2010), Minimac (Howie *et al.*, 2012), and haplotype patterns from the 1000 Genomes Project reference panel were used to impute SNP genotypes not directly assayed by the GWAS arrays. Imputation was performed as described previously (Nho *et al.*, 2013; Ramanan *et al.*, 2014b). Following additional quality control (SNP call rate < 95%, Hardy-Weinberg $P < 1 \times 10^{-6}$) and frequency filtering (MAF < 5%), 6 112 217 genotyped and imputed SNPs were

available for analysis. Six participant pairs exhibited significant relatedness (PI_HAT > 0.5) and therefore one individual from each pair was randomly selected for exclusion. For additional studies in IMAS, MAP and ROS, identical procedures were used to impute the specific SNPs required for analysis (Chibnik *et al.*, 2011; Ramanan *et al.*, 2014a).

Whole genome sequencing was obtained from blood genomic DNA samples for a subset of the ADNI sample. Sequencing was performed using the Illumina HiSeq2000 system through paired-end read chemistry and read lengths of 100 base pairs. The resulting Illumina GSEQ files were converted into FASTQ files for introductory evaluation using FastQC (Andrews, 2010). Initial alignment to the reference human genome (NCBI build 37.72) for bases with Phred quality > 15 was completed using the Burrows-Wheeler Alignment tool (Li and Durbin, 2009). Suspicious reads were locally realigned and the Illumina base calling quality scores were recalibrated to account for effects of sequencing technology and machine cycle. These realigned reads were written to a BAM file to be used for multi-sample variant calling using the GATK HaplotypeCaller (DePristo *et al.*, 2011). ANNOVAR (Wang *et al.*, 2010b) was used to annotate variants passing recommended quality criteria (Van der Auwera *et al.*, 2013). Participants with poor quality variant calls (concordance rate < 99% for SNPs genotyped through both sequencing and the Illumina HumanOmni2.5-4v1 array) were excluded from further analysis.

To limit potential effects of population stratification, all genetic analyses were restricted to non-Hispanic white participants as determined by multidimensional clustering using PLINK. To verify appropriate control for population structure, EIGENSTRAT was used to generate principal component eigenvectors for use as covariates in *post hoc* analyses.

Statistical analysis

GWAS was performed using linear regression under an additive genetic model in PLINK. Baseline age and gender were included as covariates in the GWAS. A conservative significance threshold ($P < 5 \times 10^{-8}$) was used based on a Bonferroni correction of one million independent tests (Pe'er *et al.*, 2008). Manhattan and Q-Q plots were generated with Haploview and regional association plots were generated with LocusZoom. The genome partitioning algorithm GCTA (Yang *et al.*, 2011) was used to estimate the proportion of phenotypic variance explained by all SNPs in the GWAS. Power calculations and curves were obtained using GWAPower (Feng *et al.*, 2011).

Significant associations were further investigated using sequence data from a subset of the GWAS sample. Common variants in *IL1RAP*, defined as having $MAF \geqslant 1/\sqrt{(2n)} = 0.034$ (Ionita-Laza *et al.*, 2013), were analysed using linear regression under an additive genetic model in PLINK. SKAT (Ionita-Laza *et al.*, 2013) was used to perform association testing of low-frequency and rare *IL1RAP* variants (MAF < 0.034). Pairwise linkage disequilibrium calculations were obtained for selected SNP pairs using PLINK.

Complementary approaches were used to extend the GWAS findings. GATES (KGG software version 2.5) (Li *et al.*, 2011) was used to calculate a summary *P*-value for each gene (including a default ± 5 kb window to account for putative regulatory regions) based on its size, linkage disequilibrium

structure and constituent GWAS SNP associations. GSA-SNP (Nam *et al.*, 2010; Ramanan *et al.*, 2012a) was used to identify biological pathways exhibiting enrichment of association in the GWAS. Pathway definitions from three resources (Biocarta, KEGG and Reactome) were downloaded from the Molecular Signatures Database, version 4.0 and analysis was restricted to pathways containing 5–100 genes to limit the potential for size-influenced spurious associations (Ramanan *et al.*, 2012b). Pathways with false discovery rate (FDR)-corrected $P < 0.05$ were considered as significant.

Statistical Parametric Mapping 8 (Wellcome Trust Centre for Neuroimaging) was used to perform voxel-wise analysis of the effect of *IL1RAP* rs12053868 on longitudinal change in ^{18}F-florbetapir PET amyloid burden. A two-way ANCOVA was performed using rs12053868 genotype and scan visit (baseline versus 2-year follow-up) as the independent variables and age, gender, baseline diagnosis, *APOE* ε4 status (positive versus negative), and time between PET scans as covariates. To specify an additive model, we *a priori* (based on the GWAS results) coded the analysis vector as [positive change in AA] < [positive change in GA] < [positive change in GG], corresponding to a vector of [−1, 0, −1, 1, −1, 2]. A grey matter mask was used and results were displayed at a voxel-wise threshold of $P < 0.001$ (uncorrected) with minimum cluster size (k) = 175 voxels. These voxel-wise parameters were selected to approximately correspond to a cluster-wise threshold of $P < 0.05$ (FDR-corrected). Only the GG > GA > AA results are shown, as no significant clusters were observed from the reciprocal model of AA > GA > GG.

Additional analyses were performed using IBM SPSS Statistics, Version 22.0. Following the GWAS, *post hoc* models including additional covariates were used to assess the robustness of the association of *IL1RAP* rs12053868 with higher rates of amyloid accumulation. Baseline ^{18}F-florbetapir PET SUVR and the square of this value were both included among the additional covariates in these *post hoc* analyses to account for the sigmoidal relationship of cortical amyloid PET burden to time (Jack *et al.*, 2013b). Consistent with previous data (Jack *et al.*, 2013b), the rate of amyloid accumulation as a function of baseline amyloid burden displayed an inverted U relationship (Supplementary Fig. 1). A one-way ANCOVA was used to assess the effect of rs12053868 genotype (AA versus GA/GG) on annualized per cent change in bilateral temporal cortex thickness, including baseline age, gender, total intracranial volume, and MRI scanner type (1.5 T versus 3.0 T field strength) as covariates. A subsequent two-way ANCOVA was performed to further explore the potential interaction of rs12053868 genotype with baseline diagnosis (cognitively normal versus MCI versus Alzheimer's disease). Logistic regression was used to test the association of rs12053868 genotype (AA versus GA/GG) with progression from MCI to Alzheimer's disease, including baseline age and gender as covariates. The associations of rs12053868 with ^{11}C-PBR28 PET SUV and longitudinal change in memory performance were tested using linear regression under an additive genetic model. As described above, baseline age, gender, and *TSPO* rs6971 genotype were included as covariates in the ^{11}C-PBR28 PET analysis. Baseline age, gender, and education were included as covariates in the memory analysis. METAL (Willer *et al.*, 2010) was used to perform inverse-variance weighted meta-analysis of the within-cohort memory studies.

Results

Longitudinal change in brain amyloid PET burden in ADNI participants

Primary phenotype (annualized per cent change in global cortical amyloid burden) and GWAS data passing stringent quality control were available for 495 ADNI participants (Table 1). Baseline age and gender were included as covariates in all analyses. The annualized per cent change in cortical amyloid burden was approximately normally distributed across the full sample (Supplementary Fig. 2). Mean annualized rates of amyloid accumulation were higher in Alzheimer's disease (1.36%; $n = 41$) than in MCI (0.79%; $P = 0.02$; $n = 294$) or cognitively normal (0.66%; $P = 5.47 \times 10^{-3}$; $n = 160$) participants.

APOE ε4 is associated with higher rates of amyloid accumulation

Because of its well-known association with Alzheimer's disease, prior to GWAS we investigated the effect of the *APOE* locus on longitudinal change in amyloid burden. Genotypes for *APOE* rs429358 and rs7412 were obtained for all but one participant. *APOE* ε4 carriers showed larger increases in amyloid burden over time compared to non-carriers ($P = 9.00 \times 10^{-6}$; Cohen's $d = 0.42$; Fig. 1A). *APOE* ε2/ε3 participants displayed lower rates of amyloid accumulation compared to ε3/ε3 ($P = 0.01$; Cohen's $d = 0.41$), ε3/ε4 ($P = 1.42 \times 10^{-5}$; Cohen's $d = 0.75$), and ε4/ε4 ($P = 1.57 \times 10^{-4}$; Cohen's $d = 0.84$) participants (Fig. 1B).

GWAS of longitudinal change in amyloid PET burden

To identify additional genetic modulators of longitudinal change in amyloid burden, we performed a GWAS testing 6 112 217 SNPs, with baseline age and gender included as covariates (Fig. 2). No evidence of systematic inflation of P-values was observed ($\lambda = 1.016$; Supplementary Fig. 3).

A genome-wide significant association was identified on chromosome 3 for rs12053868, an intronic SNP in *IL1RAP* ($P = 1.38 \times 10^{-9}$; Fig. 3A). The rs12053868-G allele was associated with higher rates of amyloid accumulation compared to the major (A) allele (Fig. 3B). A large effect size was observed in homozygous GG participants (Cohen's $d = 1.20$) equivalent to an odds ratio of 8.79 (Borenstein, 2009). Using stepwise linear regression with forward selection, this SNP explained 7.1% of the phenotypic variance in addition to, and independent from, the 3.4% explained by *APOE* ε4 status (Supplementary Fig. 4). This association remained genome-wide significant ($P = 5.80 \times 10^{-9}$) after the inclusion of *APOE* ε4 status, baseline diagnosis, years of education, baseline cortical

amyloid PET burden (modelled as described in the 'Materials and methods' section), and the first three principal components from population structure analysis. No significant interactions were identified between rs12053868 and any of these factors, or age or gender. The effect of the G allele on higher rates of amyloid accumulation was present in both amyloid-negative and amyloid-positive participants as classified by the baseline PET scan (Supplementary Fig. 5). Using voxel-wise analysis to further characterize the spatial effect of this SNP in the brain, we again observed an association of rs12053868-G with higher rates of amyloid accumulation, with significant clusters for this effect observed primarily in the bilateral frontal, medial, and lateral parietal, and lateral temporal lobes, as well as throughout the posterior and anterior cingulate cortex (Fig. 3C).

Suggestive associations with longitudinal change in amyloid burden ($P < 5 \times 10^{-6}$) were also identified (Fig. 2 and Table 2). These included additional SNPs in *IL1RAP*, as well as SNPs on other chromosomes within or near *KCNG1* (potassium voltage-gated channel, subfamily G, member 1), *UBR3* (ubiquitin protein ligase E3, component n-recognin 3, putative), and *JAM2* (junctional adhesion molecule 2). Variants in *BIN1* (bridging integrator 1) and *CASS4* (cas scaffolding protein family member 4) which were identified in recent Alzheimer's disease case-control GWAS (Hollingworth *et al.*, 2011; Naj *et al.*, 2011; Lambert *et al.*, 2013) displayed uncorrected $P < 0.05$ in our analysis (Supplementary Table 1). Collectively, all SNPs tested in the GWAS (including the *IL1RAP* and *APOE* SNPs described previously) were estimated to explain 34% of the phenotypic variance based on a genome partitioning analysis (Yang *et al.*, 2011).

Table 1 Selected sample characteristics

	ADNI	IMAS[a]	MAP[b]	ROS[b]
Participants, *n*	495	25	178	190
Gender				
Male	274 (55%)	8 (32%)	54 (30%)	68 (36%)
Female	221 (45%)	17 (68%)	124 (70%)	122 (64%)
Age at baseline (years)	73.0 (7.8)	70.6 (7.3)	80.8 (6.2)	76.0 (6.8)
Education (years)	16.4 (2.7)	16.2 (2.6)	15.0 (3.0)	18.3 (3.2)

Values are *n* (percentage) or mean (SD).
[a] 11C-PBR28 PET subsample.
[b] Memory analysis subsample.

Gene- and pathway-based GWAS extensions

Using gene-based GWAS analysis, *IL1RAP* displayed genome-wide significant association with longitudinal change in amyloid burden [$P < 2.17 \times 10^{-6}$ (0.05/23 000 genes)]. Additional genes not initially uncovered through single SNP analysis displayed strong gene-level associations (Table 3). We also identified 83 biological pathways displaying enrichment of GWAS association, including numerous pathways related to cell adhesion and the complement system (Supplementary Table 2).
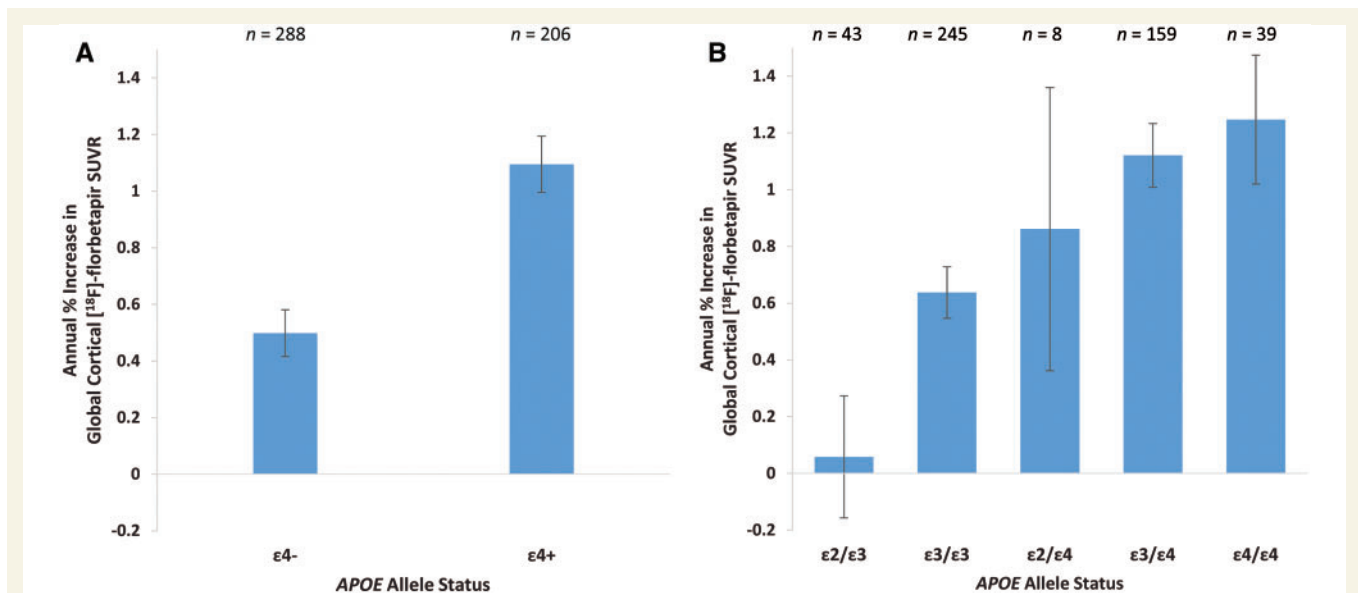

Figure 1 Effect of the *APOE* locus on 2-year change in cortical amyloid PET burden. Mean annualized per cent change in global cortical ^{18}F-florbetapir SUVR (adjusted for age and gender) $\pm$ standard errors are displayed based on (**A**) *APOE* ε4 status and (**B**) *APOE* ε2/ε3/ε4 status. (**A**) *APOE* ε4 carriers exhibited larger increases in brain amyloid PET burden compared to non-carriers ($P = 9.00 \times 10^{-6}$). (**B**) *APOE* ε2/ε3 participants displayed lower rates of amyloid accumulation compared to ε3/ε3 ($P = 0.01$), ε3/ε4 ($P = 1.42 \times 10^{-5}$), and ε4/ε4 ($P = 1.57 \times 10^{-4}$) participants.

Deep sequence analysis of *IL1RAP*

To further investigate the *IL1RAP* locus, we analysed gene sequence data for a subset of the GWAS sample (*n* = 435). Following stringent quality control, 1311 base pairs with at least one alternative allele present in the sample were available for analysis. Testing of 406 common variants confirmed a peak association with higher rates of amyloid accumulation for rs12053868 ($P = 8.18 \times 10^{-9}$; Cohen's *d* = 1.18 for GG versus AA). Although six additional common variants displayed strong association ($P < 5 \times 10^{-4}$), pairwise linkage disequilibrium calculations (Supplementary Table 3) and conditional analyses suggested that these SNPs, while not complete proxies for rs12053868, were not independent from rs12053868. Using SKAT (Ionita-Laza *et al.*, 2013), we identified a collective association of low-frequency and rare variants with rate of change in amyloid burden ($P = 7.74 \times 10^{-3}$).

IL1RAP rs12053868 is associated with a marker of cortical microglial activation

IL1RAP encodes a necessary component of the IL-1 (interleukin-1) receptor complex and its downstream signalling pathway (Gabay *et al.*, 2010). IL-1 is a potent pro-inflammatory cytokine known to promote activation of microglia, the resident phagocytes in the brain (Ghosh *et al.*, 2013; Doens and Fernandez, 2014). Recent reports have suggested that microglia may be crucial in clearing brain amyloid and limiting plaque growth (Chakrabarty *et al.*, 2015; Condello *et al.*, 2015; Johansson *et al.*, 2015). We hypothesized that the *IL1RAP* SNP associated with higher rates of amyloid accumulation would also be associated with lower microglial activation. We tested this *in vivo* in IMAS using PET and ^{11}C-PBR28, a radioligand considered to be a marker of microglial activity (Brown *et al.*, 2007). Controlling for age, gender, and *TSPO* rs6971 genotype, *IL1RAP* rs12053868-G was associated with lower cortical ^{11}C-PBR28 signal, indicative of lower cortical microglial activation ($P = 0.031$; Cohen's *d* = 1.33; Supplementary Fig. 6).

IL1RAP rs12053868-G carriers exhibit greater temporal cortex atrophy over 2 years

Amyloid deposition has been associated with increased rates of brain atrophy in cognitively normal older adults and in Alzheimer's disease (Storandt *et al.*, 2009; Chetelat *et al.*, 2010; Dore *et al.*, 2013). We hypothesized that
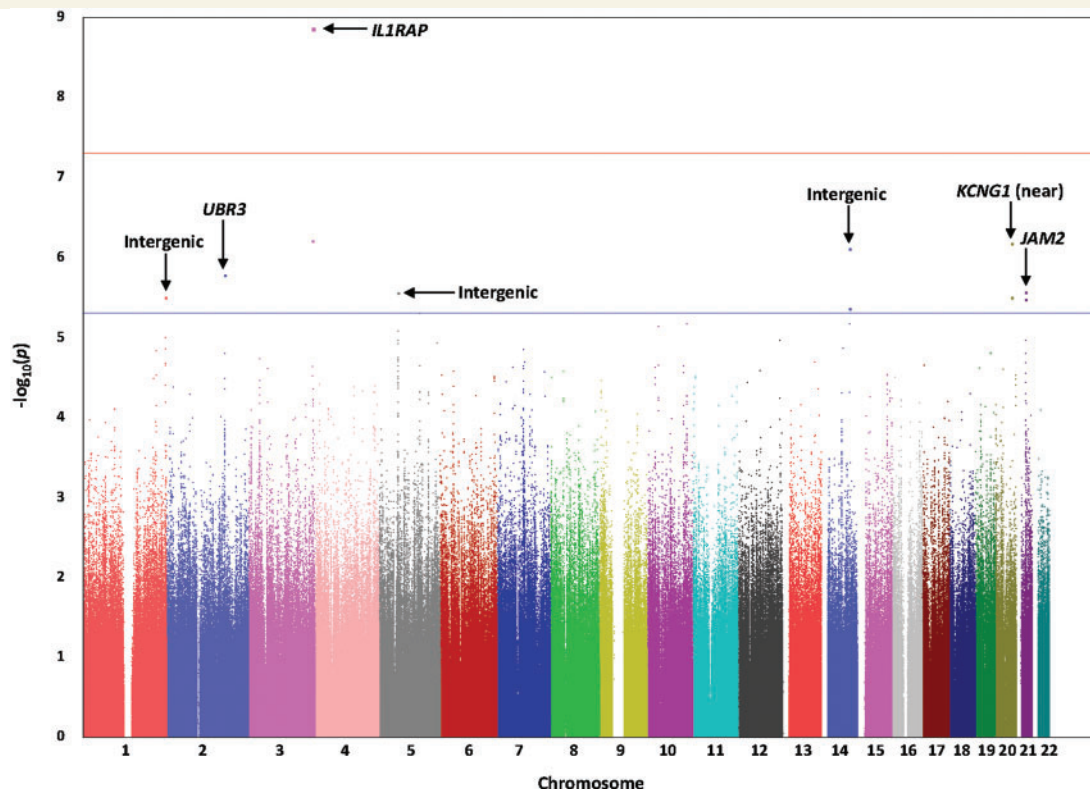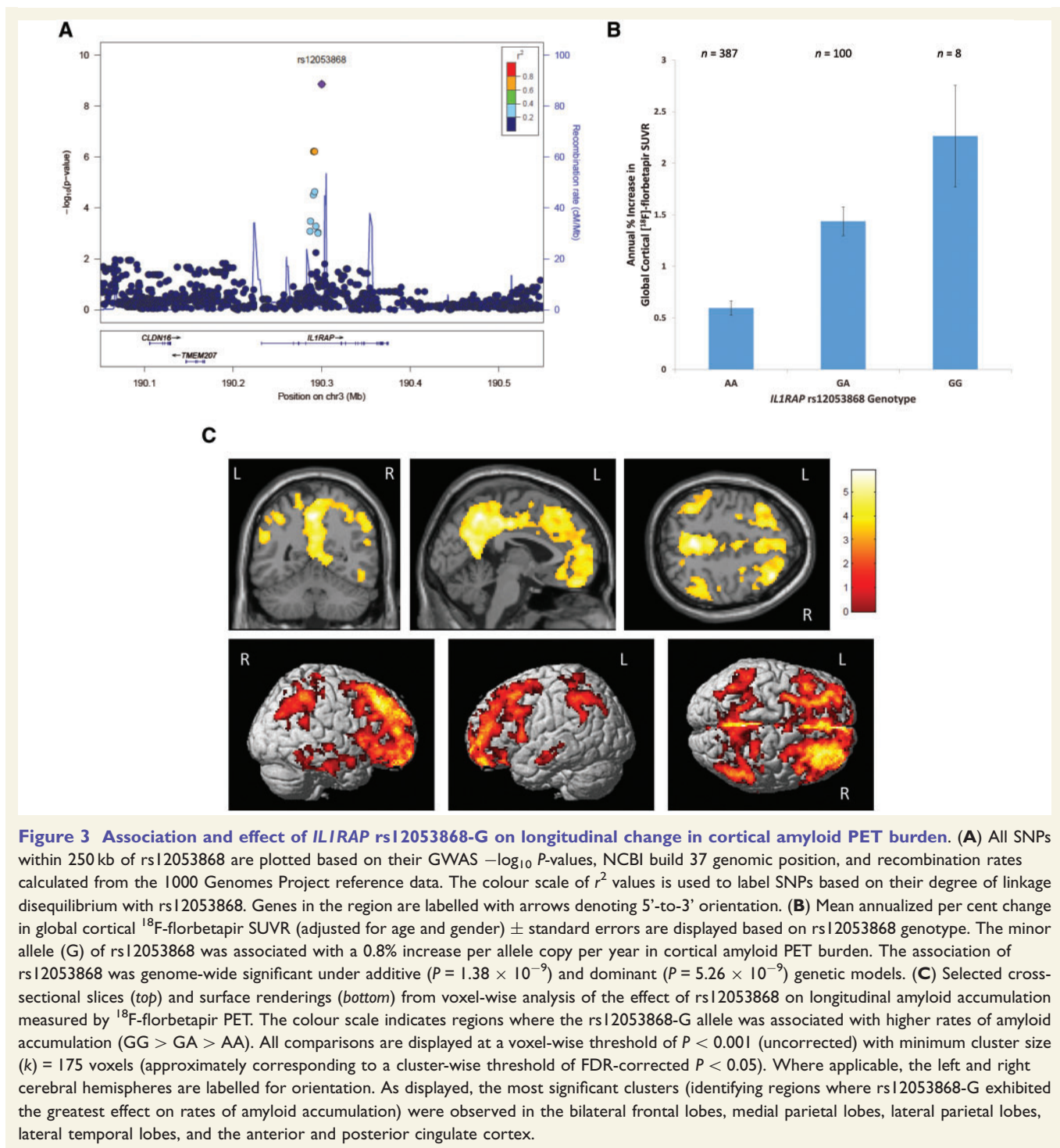

Figure 2 Manhattan plot for the GWAS of longitudinal change in cortical amyloid PET burden. Observed $-\log_{10}$ *P*-values (*y*-axis) are displayed for all tested SNPs on each autosomal chromosome (*x*-axis). A genome-wide significant association ($P < 5 \times 10^{-8}$; red line) with longitudinal change in global cortical amyloid burden measured by ^{18}F-florbetapir PET was identified on chromosome 3 within *IL1RAP*. Suggestive associations ($P < 5 \times 10^{-6}$; blue line) were identified on additional chromosomes.

Figure 3 Association and effect of *IL1RAP* rs12053868-G on longitudinal change in cortical amyloid PET burden. (**A**) All SNPs within 250 kb of rs12053868 are plotted based on their GWAS $-\log_{10}$ P-values, NCBI build 37 genomic position, and recombination rates calculated from the 1000 Genomes Project reference data. The colour scale of r^2 values is used to label SNPs based on their degree of linkage disequilibrium with rs12053868. Genes in the region are labelled with arrows denoting 5'-to-3' orientation. (**B**) Mean annualized per cent change in global cortical [18F]-florbetapir SUVR (adjusted for age and gender) $\pm$ standard errors are displayed based on rs12053868 genotype. The minor allele (G) of rs12053868 was associated with a 0.8% increase per allele copy per year in cortical amyloid PET burden. The association of rs12053868 was genome-wide significant under additive ($P = 1.38 \times 10^{-9}$) and dominant ($P = 5.26 \times 10^{-9}$) genetic models. (**C**) Selected cross-sectional slices (*top*) and surface renderings (*bottom*) from voxel-wise analysis of the effect of rs12053868 on longitudinal amyloid accumulation measured by [18F]-florbetapir PET. The colour scale indicates regions where the rs12053868-G allele was associated with higher rates of amyloid accumulation (GG > GA > AA). All comparisons are displayed at a voxel-wise threshold of $P < 0.001$ (uncorrected) with minimum cluster size (k) = 175 voxels (approximately corresponding to a cluster-wise threshold of FDR-corrected $P < 0.05$). Where applicable, the left and right cerebral hemispheres are labelled for orientation. As displayed, the most significant clusters (identifying regions where rs12053868-G exhibited the greatest effect on rates of amyloid accumulation) were observed in the bilateral frontal lobes, medial parietal lobes, lateral parietal lobes, lateral temporal lobes, and the anterior and posterior cingulate cortex.

IL1RAP rs12053868-G would be associated with higher rates of atrophy in Alzheimer's disease-specific regions (the bilateral temporal cortex) (Dore *et al.*, 2013). Using structural MRI in a subset of the GWAS sample ($n = 358$), rs12053868-G carriers exhibited greater declines in temporal cortex thickness compared to non-carriers ($P = 0.035$; Cohen's $d = 0.28$; Supplementary Fig. 7A). This effect was observed across all diagnostic groups (Supplementary Fig. 7B) and remained significant

($P = 0.042$) after the inclusion of diagnosis ($P < 0.001$) as an independent predictor variable.

IL1RAP rs12053868-G carriers exhibit greater likelihood of progression from MCI to Alzheimer's disease

Amyloid deposition in MCI is a predictor of clinical progression to Alzheimer's disease (Huijbers *et al.*, 2015).

Table 2 Peak associations ($P < 5 \times 10^{-6}$) for the GWAS of longitudinal change in amyloid PET burden

Chromosome	SNP	Gene symbol	Gene name	MAF[a]	β (SE)[b]	R^{2c}	P	Gen/Imp[d]
3	rs12053868	*IL1RAP*	Interleukin-1 receptor accessory protein	0.12	0.84 (0.14)	0.071	1.38×10^{-9}	437/58
3	rs3773970	*IL1RAP*	Interleukin-1 receptor accessory protein	0.13	0.67 (0.13)	0.049	6.19×10^{-7}	494/1
3	rs3773973	*IL1RAP*	Interleukin-1 receptor accessory protein	0.13	0.67 (0.13)	0.049	6.19×10^{-7}	436/59
3	rs147346019	*IL1RAP*	Interleukin-1 receptor accessory protein	0.13	0.67 (0.13)	0.049	6.19×10^{-7}	0/495
20	rs10470013	Near *KCNG1*	Potassium voltage-gated channel, subfamily G, member 1	0.11	0.73 (0.14)	0.049	6.65×10^{-7}	438/57
14	rs79110742	Intergenic		0.06	0.94 (0.19)	0.048	7.74×10^{-7}	0/495
2	rs13012722	*UBR3*	Ubiquitin protein ligase E3 component n-recognin 3 (putative)	0.49	−0.45 (0.09)	0.045	1.67×10^{-7}	0/495
21	rs8129913	*JAM2*	Junctional adhesion molecule 2	0.43	0.43 (0.09)	0.043	2.75×10^{-6}	0/495
21	rs11087971	*JAM2*	Junctional adhesion molecule 2	0.43	0.43 (0.09)	0.043	2.75×10^{-6}	0/495
5	rs11744848	Intergenic		0.13	−0.63 (0.13)	0.043	2.80×10^{-6}	0/495
1	rs10737896	Intergenic		0.21	−0.51 (0.11)	0.043	3.19×10^{-6}	0/495
1	rs7534801	Intergenic		0.21	−0.51 (0.11)	0.043	3.19×10^{-6}	495/0
20	rs6096218	Near *KCNG1*	Potassium voltage-gated channel, subfamily G, member 1	0.11	0.69 (0.15)	0.043	3.20×10^{-6}	494/1
21	rs4817054	*JAM2*	Junctional adhesion molecule 2	0.43	0.43 (0.09)	0.043	3.34×10^{-6}	0/495
14	rs8023225	Intergenic		0.08	0.77 (0.17)	0.042	4.41×10^{-6}	494/1

[a]Minor allele frequency in the GWAS sample.
[b]β (unstandardized) effect size from the GWAS (with standard error indicated in parentheses), denoting the annualized percent change in global cortical ^{18}F-florbetapir SUVR conferred by one copy of the minor allele.
[c]Proportion of phenotypic variance explained (not necessarily uniquely) by the SNP, including age and gender as covariates.
[d]Gen = number of participants for which the SNP was genotyped on a GWAS array (ADNI participants were genotyped on one of three Illumina GWAS arrays which each had different genomic coverages); Imp = number of participants for which the SNP was imputed.

We hypothesized that rs12053868-G would be associated with a greater likelihood of progression from MCI to Alzheimer's disease. Within the GWAS sample, 269/294 participants diagnosed with MCI at baseline had diagnosis information at 2-year follow-up, including 42 who progressed to clinical Alzheimer's disease and 227 who did not. Using logistic regression with age and gender included as covariates, rs12053868-G carriers were more likely to convert to Alzheimer's disease within the follow-up period than non-carriers [$P = 0.025$, odds ratio (OR) = 2.32 (1.11–4.87)] (Supplementary Fig. 8).

IL1RAP rs12053868 is associated with accelerated cognitive decline in high risk individuals

Memory impairment is the cardinal early symptom of Alzheimer's disease (Ballard *et al.*, 2011) and amyloid deposition is known to be related to memory impairment and longitudinal cognitive decline (Sperling *et al.*, 2013; Villemagne *et al.*, 2013). We hypothesized that rs12053868-G would be associated with accelerated decline of memory in participants at high risk for amyloid pathology (defined as being *APOE* ε4 positive or having a baseline diagnosis of clinical Alzheimer's disease). In a meta-analysis of 579 participants from three independent cohorts (ADNI, MAP and ROS), rs12053868-G was associated with faster 2-year decline in verbal episodic memory performance ($P = 7.72 \times 10^{-4}$), with each copy of the G

allele adding approximately one-quarter of a standard deviation to the rate of decline (Supplementary Fig. 9). The heterogeneity statistic ($I^2 = 0$, $P = 0.37$) indicated no significant heterogeneity across the individual cohort studies used for meta-analysis (Higgins *et al.*, 2003).

Discussion

To our knowledge, this is the first reported GWAS of longitudinal change in brain amyloid load measured by ^{18}F-florbetapir PET. Our findings support *IL1RAP* as a novel potential Alzheimer's disease target and highlight the use of amyloid PET as a valuable Alzheimer's disease endophenotype, particularly in a longitudinal framework.

IL1RAP encodes a necessary and potentially rate-limiting component of the pro-inflammatory IL-1 signalling pathway (Gabay *et al.*, 2010). Activation of this pathway requires binding of IL1RAP to the IL-1/IL-1 receptor complex (Wang *et al.*, 2010a). *IL1RAP* splice variants, including one isoform expressed only in the CNS as well as a different soluble variant, exert inhibitory effects on the IL-1 pathway (Smith *et al.*, 2009). More broadly, the IL-1 pathway and its component genes have long been foci of interest in genetic and other studies of the Alzheimer's disease spectrum (Green *et al.*, 2002; Wang *et al.*, 2005; Tsai *et al.*, 2010; Latz *et al.*, 2013). These studies, and recent findings from Alzheimer's disease mouse models revealing that IL-1 overexpression leads to increased plaque-associated activated microglia, decreased amyloid burden, and

Table 3 Peak GATES gene-based associations with longitudinal change in amyloid PET burden

Chromosome	Gene symbol	Gene name	GATES P
3	IL1RAP	Interleukin-1 receptor accessory protein	9.45×10^{-8}
20	PSMA7	Proteasome subunit, alpha type, 7	1.33×10^{-4}
20	LSM14B	SCD6 homolog B (S. cerevisiae)	1.46×10^{-4}
21	JAM2	Junctional adhesion molecule 2	1.59×10^{-4}
19	APOC1	Apolipoprotein C1	1.74×10^{-4}
2	UBR3	Ubiquitin protein ligase E3 component n-recognin 3 (putative)	1.75×10^{-4}
19	APOE	Apolipoprotein E	2.26×10^{-4}
10	PNLIPRP1	Pancreatic lipase-related protein 1	2.33×10^{-4}
19	TOMM40	Translocase of outer mitochondrial membrane 40 homolog (yeast)	3.10×10^{-4}
3	MIR6828	MicroRNA 6828	3.12×10^{-4}
14	SNAPC1	Small nuclear RNA activating complex, polypeptide 1	3.47×10^{-4}
12	BRI3BP	Brain protein I3 binding protein	3.82×10^{-4}
20	SS18L1	Synovial sarcoma translocation gene on chromosome 18-like 1	4.09×10^{-4}
3	CLDN11	Claudin 11	4.98×10^{-4}

increased tau phosphorylation (Prinz *et al.*, 2011; Ghosh *et al.*, 2013) highlight the potentially crucial roles of the IL-1/IL1RAP pathway in modulating Alzheimer's disease pathology.

Microglial activation pathways are leading candidates for promoting amyloid clearance and limiting plaque development. Variants in *TREM2* (triggering receptor expressed on myeloid cells 2) thought to impair microglial phagocytic function have been associated with increased Alzheimer's disease risk (Guerreiro *et al.*, 2013; Jonsson *et al.*, 2013) and large-scale pathway and network analyses have also implicated activated microglia in Alzheimer's disease pathogenesis (Jones *et al.*, 2010; Zhang *et al.*, 2013). Along with recent studies relating loss of microglial function to worsening amyloid pathology (Bradshaw *et al.*, 2013; Chakrabarty *et al.*, 2015; Condello *et al.*, 2015; Johansson *et al.*, 2015), the discovery that *IL1RAP* is associated with higher rates of amyloid accumulation and lower signal of a PET marker for microglial activation provides strong reinforcement for this hypothesis.

IL1RAP is a known therapeutic target for leukaemia (Barreyro *et al.*, 2012; Askmyr *et al.*, 2013) and chronic inflammatory diseases such as rheumatoid arthritis (Gabay *et al.*, 2010; Dinarello, 2011). Pathway analysis of a large Alzheimer's disease case-control GWAS (Harold *et al.*, 2009) ($n = 11\,789$) identified association of immune-related pathways with a significant contribution from *IL1RAP*, including a top Alzheimer's disease risk SNP (rs4571225; $P = 1.26 \times 10^{-5}$) which is not a proxy for, but is in moderate linkage disequilibrium with rs12053868 ($r^2 = 0.003$; $D' = 0.63$) (Jones *et al.*, 2010). An intergenic SNP (rs9877502) 290 kb downstream of *IL1RAP* also displayed genome-wide significant association with cross-sectional CSF tau levels (Cruchaga *et al.*, 2013), but this SNP is not in linkage disequilibrium with rs12053868 ($r^2 = 0.003$; $D' = 0.10$). Prior to our study, *IL1RAP* rs12053868 had not been previously reported in an

Alzheimer's disease genetic association study. Our new association for this SNP may reflect a relative specificity for amyloid accumulation versus the more heterogeneous case-control status (Kendler and Neale, 2010), increased power obtained via endophenotype analysis (Potkin *et al.*, 2009), or previous suggestive association below reporting thresholds.

IL1RAP is highly expressed in the brain but seems to be downregulated in prefrontal cortex with increasing age (Kang *et al.*, 2011; Primiani *et al.*, 2014). Although it is not a coding SNP, rs12053868 may be associated with decreased *IL1RAP* expression in the cortex and hippocampus based on preliminary data (Supplementary Fig. 10). There is substantial precedent for non-coding SNPs to have functional effects (Kapranov *et al.*, 2007; Consortium, 2012; De Jager *et al.*, 2014), and intronic *IL1RAP* SNPs have previously been associated with plasma levels of soluble IL1RAP, including a top SNP (rs724608; $P = 8.81 \times 10^{-13}$) which is in moderate linkage disequilibrium with rs12053868 ($r^2 = 0.005$; $D' = 0.45$) (Lourdusamy *et al.*, 2012). However, functional genomics studies in brain tissue will be needed to further characterize the *IL1RAP* locus and its potential impact on Alzheimer's disease pathogenesis.

Following the GWAS discovery, we related *IL1RAP* rs12053868-G to other longitudinal Alzheimer's disease endophenotypes. In particular, the observed effect of rs12053868 on clinical progression in MCI argues for further study of the impact of *IL1RAP* on clinical trajectories in pre-MCI states. This result also suggests that in combination with *APOE*, other known Alzheimer's disease risk genes, and family history, *IL1RAP* might be useful for risk enrichment in clinical trial design and risk stratification in study analysis or as part of personalized genetic susceptibility tests for Alzheimer's disease onset or progression.

Using gene sequence data from a subset of the GWAS sample, we identified a pooled association of low-frequency

and rare *IL1RAP* variants with the rate of amyloid accumulation. Although larger samples will facilitate assessment of the effects of individual rare variants, this finding bolsters the initial GWAS discovery of *IL1RAP*, as genes truly related to disease pathogenesis are likely to contain associated common and rare variants (Zuk *et al.*, 2014).

Suggestive associations were identified through GWAS and may have reached genome-wide significance with a larger sample. These included SNPs in *JAM2*, adjacent to *APP* on chromosome 21. Mutations in *APP* are among the causes of early-onset Alzheimer's disease (Bettens *et al.*, 2013) and a rare variant in *APP* was found to be protective against late-onset Alzheimer's disease (Jonsson *et al.*, 2012). SNPs near *APP* were also associated with amyloid plaque burden in a neuropathological study of post-mortem brain tissue (Shulman *et al.*, 2013). Notably, the top SNP from that study (rs2829887) is in strong linkage disequilibrium with the top *JAM2* SNP (rs8129913) from our analysis of longitudinal amyloid PET ($r^2 = 0.57$; $D' = 0.91$). In addition, *JAM2* ($P = 1.59 \times 10^{-4}$) and *APP* ($P = 0.048$) each displayed uncorrected gene-level $P < 0.05$ in our study. These suggestive findings argue for further investigation of the *JAM2-APP* locus to clarify the potential functional gene(s) and causal variant(s) related to amyloid pathology.

Complementary gene- and pathway-based analyses were used to test for collective effects of multiple variants within shared functional units (Ramanan *et al.*, 2012*b*). Gene-based analysis uniquely identified additional candidates for further study, and enrichment of GWAS association was identified in pathways related to the complement system, cell adhesion, and *Notch* transcription, as well as the IL-1 pathway overall. Activation of cell adhesion and complement receptors are crucial for microglia to recognize, aggregate around, and ultimately clear amyloid deposits (Ramanan and Saykin, 2013; Doens and Fernandez, 2014). Notch has key roles in regulating neuronal plasticity but these activities depend on its initial cleavage by γ-secretase, the enzyme also responsible for generating amyloid-β (Mattson, 2003).

All SNPs tested in the GWAS were estimated to collectively explain 34% of the variance in 2-year change in brain amyloid PET burden, a considerable proportion given the modest sample used for GWAS. Although amyloid deposition and clearance are dynamic processes with unknown heritability, our findings indicate that the rate of amyloid accumulation has a substantial genetic component and suggest that additional genetic variants, as well as gene–gene and gene–environment interactions, may be discovered in future using larger samples and complementary analytical approaches.

This work has several limitations. Although we leveraged publicly available ADNI genetics and longitudinal amyloid PET data to perform this original study, our sample size had limited power for a GWAS (Supplementary Fig. 11). The future availability of comparable data from larger samples will allow for suitable replication testing and additional discovery. Functional genomics experiments not performed here, including microglial immunohistochemistry and analyses of *IL1RAP* knockout and antibody- and siRNA-based knockdown models, will also be needed to characterize our novel finding. In particular, studies of brain tissue, rather than blood genomic DNA, will be better able to assess for epigenetic and transcriptomic events that may elucidate the mechanistic relationship between *IL1RAP* and amyloid accumulation. Further, while it could not be appropriately addressed with presently available data, analyses of serial CSF samples would help assess whether *IL1RAP* impacts soluble and oligomeric forms of amyloid. Finally, candidate PET radiotracers selective for tau aggregation in the brain are also now in clinical trials (Villemagne *et al.*, 2015), and if validated, would aid investigation of the potential relationship between the IL-1/ IL1RAP pathway and tau pathology.

In conclusion, we discovered a new association of *IL1RAP* rs12053868 with higher rates of amyloid accumulation on longitudinal ^{18}F-florbetapir PET and we related this SNP to other Alzheimer's disease endophenotypes, including clinical progression, cognitive decline, temporal cortex atrophy on MRI, and lower signal of a PET marker of microglial activation. The biological roles of *IL1RAP* in amyloid deposition and clearance, particularly in relation to microglial function, merit further investigation and may have significant implications for risk stratification and therapeutic development in Alzheimer's disease.

Funding

Supplementary material

Supplementary material is available at *Brain* online.

References

Andrews S FastQC: a quality-control tool for high-throughput sequence data. http://wwwbioinformaticsbabrahamacuk/projects/fastqc. 2010.

Askmyr M, Agerstam H, Hansen N, Gordon S, Arvanitakis A, Rissler M, et al. Selective killing of candidate AML stem cells by antibody targeting of IL1RAP. Blood 2013; 121: 3709–13.

Ballard C, Gauthier S, Corbett A, Brayne C, Aarsland D, Jones E. Alzheimer's disease. Lancet 2011; 377: 1019–31.

Barreyro L, Will B, Bartholdy B, Zhou L, Todorova TI, Stanley RF, et al. Overexpression of IL-1 receptor accessory protein in stem and progenitor cells and outcome correlation in AML and MDS. Blood 2012; 120: 1290–8.

Bennett DA, Schneider JA, Arvanitakis Z, Wilson RS. Overview and findings from the religious orders study. Curr Alzheimer Res 2012a; 9: 628–45.

Bennett DA, Schneider JA, Buchman AS, Barnes LL, Boyle PA, Wilson RS. Overview and findings from the rush memory and aging project. Curr Alzheimer Res 2012b; 9: 646–63.

Bettens K, Sleegers K, Van Broeckhoven C. Genetic insights in Alzheimer's disease. Lancet Neurol 2013; 12: 92–104.

Borenstein M. Introduction to meta-analysis. Chichester, UK: John Wiley & Sons; 2009.

Bradshaw EM, Chibnik LB, Keenan BT, Ottoboni L, Raj T, Tang A, et al. CD33 Alzheimer's disease locus: altered monocyte function and amyloid biology. Nat Neurosci 2013; 16: 848–50.

Brown AK, Fujita M, Fujimura Y, Liow JS, Stabin M, Ryu YH, et al. Radiation dosimetry and biodistribution in monkey and man of 11C-PBR28: a PET radioligand to image inflammation. J Nucl Med 2007; 48: 2072–9.

Chakrabarty P, Li A, Ceballos-Diaz C, Eddy JA, Funk CC, Moore B, et al. IL-10 Alters immunoproteostasis in APP mice, increasing plaque burden and worsening cognitive behavior. Neuron 2015; 85: 519–33.

Chetelat G, Villemagne VL, Bourgeat P, Pike KE, Jones G, Ames D, et al. Relationship between atrophy and beta-amyloid deposition in Alzheimer disease. Ann Neurol 2010; 67: 317–24.

Chibnik LB, Shulman JM, Leurgans SE, Schneider JA, Wilson RS, Tran D, et al. CR1 is associated with amyloid plaque burden and age-related cognitive decline. Ann Neurol 2011; 69: 560–9.

Clark CM, Pontecorvo MJ, Beach TG, Bedell BJ, Coleman RE, Doraiswamy PM, et al. Cerebral PET with florbetapir compared with neuropathology at autopsy for detection of neuritic amyloid-β plaques: a prospective cohort study. Lancet Neurol 2012; 11: 669–78.

Condello C, Yuan P, Schain A, Grutzendler J. Microglia constitute a barrier that prevents neurotoxic protofibrillar Abeta42 hotspots around plaques. Nat Commun 2015; 6: 6176.

Consortium EP. An integrated encyclopedia of DNA elements in the human genome. Nature 2012; 489: 57–74.

Corder EH, Saunders AM, Strittmatter WJ, Schmechel DE, Gaskell PC, Small GW, et al. Gene dose of apolipoprotein E type 4 allele and the risk of Alzheimer's disease in late onset families. Science 1993; 261: 921–3.

Cruchaga C, Kauwe JS, Harari O, Jin SC, Cai Y, Karch CM, et al. GWAS of cerebrospinal fluid tau levels identifies risk variants for Alzheimer's disease. Neuron 2013; 78: 256–68.

De Jager PL, Srivastava G, Lunnon K, Burgess J, Schalkwyk LC, Yu L, et al. Alzheimer's disease: early alterations in brain DNA methylation at ANK1, BIN1, RHBDF2 and other loci. Nat Neurosci 2014; 17: 1156–63.

DePristo MA, Banks E, Poplin R, Garimella KV, Maguire JR, Hartl C, et al. A framework for variation discovery and genotyping using next-generation DNA sequencing data. Nat Genet 2011; 43: 491–8.

Dinarello CA. Interleukin-1 in the pathogenesis and treatment of inflammatory diseases. Blood 2011; 117: 3720–32.

Doens D, Fernandez PL. Microglia receptors and their implications in the response to amyloid beta for Alzheimer's disease pathogenesis. J Neuroinflam 2014; 11: 48.

Doraiswamy PM, Sperling RA, Johnson K, Reiman EM, Wong TZ, Sabbagh MN, et al. Florbetapir F 18 amyloid PET and 36-month cognitive decline: a prospective multicenter study. Mol Psychiatry 2014; 19: 1044–51.

Dore V, Villemagne VL, Bourgeat P, Fripp J, Acosta O, Chetelat G, et al. Cross-sectional and longitudinal analysis of the relationship between abeta deposition, cortical thickness, and memory in cognitively unimpaired individuals and in Alzheimer disease. JAMA Neurol 2013: 1–9.

Feng S, Wang S, Chen CC, Lan L. GWAPower: a statistical power calculation software for genome-wide association studies with quantitative traits. BMC Genet 2011; 12: 12.

Gabay C, Lamacchia C, Palmer G. IL-1 pathways in inflammation and human diseases. Nat Rev Rheumatol 2010; 6: 232–41.

Ghosh S, Wu MD, Shaftel SS, Kyrkanides S, LaFerla FM, Olschowka JA, et al. Sustained interleukin-1beta overexpression exacerbates tau

pathology despite reduced amyloid burden in an Alzheimer's mouse model. J Neurosci 2013; 33: 5053–64.

Green EK, Harris JM, Lemmon H, Lambert JC, Chartier-Harlin MC, St Clair D, et al. Are interleukin-1 gene polymorphisms risk factors or disease modifiers in AD?. Neurology 2002; 58: 1566–8.

Guerreiro R, Wojtas A, Bras J, Carrasquillo M, Rogaeva E, Majounie E, et al. TREM2 variants in Alzheimer's disease. N Engl J Med 2013; 368: 117–27.

Harold D, Abraham R, Hollingworth P, Sims R, Gerrish A, Hamshere ML, et al. Genome-wide association study identifies variants at CLU and PICALM associated with Alzheimer's disease. Nat Genet 2009; 41: 1088–93.

Higgins JP, Thompson SG, Deeks JJ, Altman DG. Measuring inconsistency in meta-analyses. BMJ 2003; 327: 557–60.

Hollingworth P, Harold D, Sims R, Gerrish A, Lambert JC, Carrasquillo MM, et al. Common variants at ABCA7, MS4A6A/MS4A4E, EPHA1, CD33 and CD2AP are associated with Alzheimer's disease. Nat Genet 2011; 43: 429–35.

Howie B, Fuchsberger C, Stephens M, Marchini J, Abecasis GR. Fast and accurate genotype imputation in genome-wide association studies through pre-phasing. Nat Genet 2012; 44: 955–9.

Huijbers W, Mormino EC, Schultz AP, Wigman S, Ward AM, Larvie M, et al. Amyloid-beta deposition in mild cognitive impairment is associated with increased hippocampal activity, atrophy and clinical progression. Brain 2015; 138: 1023–35.

Ionita-Laza I, Lee S, Makarov V, Buxbaum JD, Lin X. Sequence kernel association tests for the combined effect of rare and common variants. Am J Hum Genet 2013; 92: 841–53.

Jack CR, Jr, Knopman DS, Jagust WJ, Petersen RC, Weiner MW, Aisen PS, et al. Tracking pathophysiological processes in Alzheimer's disease: an updated hypothetical model of dynamic biomarkers. Lancet Neurol 2013a; 12: 207–16.

Jack CR, Jr, Wiste HJ, Lesnick TG, Weigand SD, Knopman DS, Vemuri P, et al. Brain beta-amyloid load approaches a plateau. Neurology 2013b; 80: 890–6.

Jagust WJ, Bandy D, Chen K, Foster NL, Landau SM, Mathis CA, et al. The Alzheimer's Disease Neuroimaging Initiative positron emission tomography core. Alzheimers Dement 2010; 6: 221–9.

Johansson JU, Woodling NS, Wang Q, Panchal M, Liang X, Trueba-Saiz A, et al. Prostaglandin signaling suppresses beneficial microglial function in Alzheimer's disease models. J Clin Invest 2015; 125: 350–64.

Jones L, Holmans PA, Hamshere ML, Harold D, Moskvina V, Ivanov D, et al. Genetic evidence implicates the immune system and cholesterol metabolism in the aetiology of Alzheimer's disease. PLoS One 2010; 5: e13950.

Jonsson T, Atwal JK, Steinberg S, Snaedal J, Jonsson PV, Bjornsson S, et al. A mutation in APP protects against Alzheimer's disease and age-related cognitive decline. Nature 2012; 488: 96–9.

Jonsson T, Stefansson H, Steinberg S, Jonsdottir I, Jonsson PV, Snaedal J, et al. Variant of TREM2 associated with the risk of Alzheimer's disease. N Engl J Med 2013; 368: 107–16.

Kang HJ, Kawasawa YI, Cheng F, Zhu Y, Xu X, Li M, et al. Spatiotemporal transcriptome of the human brain. Nature 2011; 478: 483–9.

Kapranov P, Willingham AT, Gingeras TR. Genome-wide transcription and the implications for genomic organization. Nat Rev Genet 2007; 8: 413–23.

Karran E, Mercken M, De Strooper B. The amyloid cascade hypothesis for Alzheimer's disease: an appraisal for the development of therapeutics. Nat Rev Drug Discov 2011; 10: 698–712.

Kendler KS, Neale MC. Endophenotype: a conceptual analysis. Mol Psychiatry 2010; 15: 789–97.

Kim J, Basak JM, Holtzman DM. The role of apolipoprotein E in Alzheimer's disease. Neuron 2009; 63: 287–303.

Kreisl WC, Jenko KJ, Hines CS, Lyoo CH, Corona W, Morse CL, et al. A genetic polymorphism for translocator protein 18 kDa

affects both *in vitro* and *in vivo* radioligand binding in human brain to this putative biomarker of neuroinflammation. J Cereb Blood Flow Metab 2013; 33: 53–8.

Lambert JC, Ibrahim-Verbaas CA, Harold D, Naj AC, Sims R, Bellenguez C, et al. Meta-analysis of 74,046 individuals identifies 11 new susceptibility loci for Alzheimer's disease. Nat Genet 2013; 45: 1452–8.

Latz E, Xiao TS, Stutz A. Activation and regulation of the inflammasomes. Nat Rev Immunol 2013; 13: 397–411.

Li H, Durbin R. Fast and accurate short read alignment with Burrows-Wheeler transform. Bioinformatics 2009; 25: 1754–60.

Li MX, Gui HS, Kwan JSH, Sham PC. GATES: a rapid and powerful gene-based association test using extended simes procedure. Am J Hum Genet 2011; 88: 283–93.

Li Y, Willer CJ, Ding J, Scheet P, Abecasis GR. MaCH: using sequence and genotype data to estimate haplotypes and unobserved genotypes. Genet Epidemiol 2010; 34: 816–34.

Lim YY, Villemagne VL, Laws SM, Pietrzak RH, Snyder PJ, Ames D, et al. APOE and BDNF polymorphisms moderate amyloid beta-related cognitive decline in preclinical Alzheimer's disease. Mol Psychiatry 2014. doi: 10.1038/mp.2014.123

Lourdusamy A, Newhouse S, Lunnon K, Proitsi P, Powell J, Hodges A, et al. Identification of cis-regulatory variation influencing protein abundance levels in human plasma. Hum Mol Genet 2012; 21: 3719–26.

Mattson MP. Neurobiology: Ballads of a protein quartet. Nature 2003; 422: 385–7.

Naj AC, Jun G, Beecham GW, Wang L-S, Vardarajan BN, Buros J, et al. Common variants at MS4A4/MS4A6E, CD2AP, CD33 and EPHA1 are associated with late-onset Alzheimer's disease. Nat Genet 2011; 43: 436–41.

Nam D, Kim J, Kim SY, Kim S. GSA-SNP: a general approach for gene set analysis of polymorphisms. Nucleic Acids Res 2010; 38: W749–54.

Nho K, Corneveaux JJ, Kim S, Lin H, Risacher SL, Shen L, et al. Whole-exome sequencing and imaging genetics identify functional variants for rate of change in hippocampal volume in mild cognitive impairment. Mol Psychiatry 2013; 18: 781–7.

Pe'er I, Yelensky R, Altshuler D, Daly MJ. Estimation of the multiple testing burden for genomewide association studies of nearly all common variants. Genet Epidemiol 2008; 32: 381–5.

Potkin SG, Turner JA, Guffanti G, Lakatos A, Torri F, Keator DB, et al. Genome-wide strategies for discovering genetic influences on cognition and cognitive disorders: methodological considerations. Cogn Neuropsychiatry 2009; 14: 391–418.

Primiani CT, Ryan VH, Rao JS, Cam MC, Ahn K, Modi HR, et al. Coordinated gene expression of neuroinflammatory and cell signaling markers in dorsolateral prefrontal cortex during human brain development and aging. PLoS One 2014; 9: e110972.

Prinz M, Priller J, Sisodia SS, Ransohoff RM. Heterogeneity of CNS myeloid cells and their roles in neurodegeneration. Nat Neurosci 2011; 14: 1227–35.

Ramanan VK, Kim S, Holohan K, Shen L, Nho K, Risacher SL, et al. Genome-wide pathway analysis of memory impairment in the Alzheimer's Disease Neuroimaging Initiative (ADNI) cohort implicates gene candidates, canonical pathways, and networks. Brain Imaging Behav 2012a; 6: 634–48.

Ramanan VK, Nho K, Shen L, Risacher SL, Kim S, McDonald BC, et al. FASTKD2 is associated with memory and hippocampal structure in older adults. Mol Psychiatry 2014a. doi: 10.1038/mp.2014.142

Ramanan VK, Risacher SL, Nho K, Kim S, Swaminathan S, Shen L, et al. APOE and BCHE as modulators of cerebral amyloid deposition: a florbetapir PET genome-wide association study. Mol Psychiatry 2014b; 19: 351–7.

Ramanan VK, Saykin AJ. Pathways to neurodegeneration: mechanistic insights from GWAS in Alzheimer's disease, Parkinson's disease, and related disorders. Am J Neurodegener Dis 2013; 2: 145–75.

Ramanan VK, Shen L, Moore JH, Saykin AJ. Pathway analysis of genomic data: concepts, methods, and prospects for future development. Trends Genet 2012b; 28: 323–32.

Rhinn H, Fujita R, Qiang L, Cheng R, Lee JH, Abeliovich A. Integrative genomics identifies APOE epsilon4 effectors in Alzheimer's disease. Nature 2013; 500: 45–50.

Risacher SL, Kim S, Nho K, Foroud T, Shen L, Petersen RC, et al. APOE effect on Alzheimer's disease biomarkers in older adults with significant memory concern. Alzheimers Dement 2015. doi: 10.1016/j.jalz.2015.03.003

Risacher SL, Shen L, West JD, Kim S, McDonald BC, Beckett LA, et al. Longitudinal MRI atrophy biomarkers: relationship to conversion in the ADNI cohort. Neurobiol Aging 2010; 31: 1401–18.

Saykin AJ, Shen L, Foroud TM, Potkin SG, Swaminathan S, Kim S, et al. Alzheimer's Disease Neuroimaging Initiative biomarkers as quantitative phenotypes: genetics core aims, progress, and plans. Alzheimers Dement 2010; 6: 265–73.

Saykin AJ, Shen L, Xiaohui Y, Kim S, Nho K, Risacher SL, et al. Genetic studies of quantitative MCI and AD phenotypes in ADNI: progress, opportunities, and plan. Alzheimers Dement 2015; 11: 792–814.

Schmidt ME, Chiao P, Klein G, Matthews D, Thurfjell L, Cole PE, et al. The influence of biological and technical factors on quantitative analysis of amyloid PET: points to consider and recommendations for controlling variability in longitudinal data. Alzheimers Dement 2014. doi: 10.1016/j.jalz.2014.09.004

Shulman JM, Chen K, Keenan BT, Chibnik LB, Fleisher A, Thiyyagura P, et al. Genetic susceptibility for Alzheimer disease neuritic plaque pathology. JAMA Neurol 2013; 70: 1150–7.

Smith DE, Lipsky BP, Russell C, Ketcham RR, Kirchner J, Hensley K, et al. A central nervous system-restricted isoform of the interleukin-1 receptor accessory protein modulates neuronal responses to interleukin-1. Immunity 2009; 30: 817–31.

Sperling RA, Johnson KA, Doraiswamy PM, Reiman EM, Fleisher AS, Sabbagh MN, et al. Amyloid deposition detected with florbetapir F 18 ((18)F-AV-45) is related to lower episodic memory performance in clinically normal older individuals. Neurobiol Aging 2013; 34: 822–31.

Storandt M, Mintun MA, Head D, Morris JC. Cognitive decline and brain volume loss as signatures of cerebral amyloid-beta peptide deposition identified with Pittsburgh compound B: cognitive decline associated with Abeta deposition. Arch Neurol 2009; 66: 1476–81.

Swaminathan S, Shen L, Risacher SL, Yoder KK, West JD, Kim S, et al. Amyloid pathway-based candidate gene analysis of [(11)C]PiB-PET in the Alzheimer's Disease Neuroimaging Initiative (ADNI) cohort. Brain Imaging Behav 2012; 6: 1–15.

Tsai S-J, Hong C-J, Liu M-E, Hou S-J, Yen F-C, Hsieh C-H, et al. Interleukin-1 beta (C-511T) genetic polymorphism is associated with cognitive performance in elderly males without dementia. Neurobiol Aging 2010; 31: 1950–5.

Van der Auwera GA, Carneiro MO, Hartl C, Poplin R, Del Angel G, Levy-Moonshine A, et al. From FastQ data to high confidence variant calls: the Genome Analysis Toolkit best practices pipeline. Curr Protoc Bioinform 2013; 11: 11.10.1–33.

Villemagne VL, Burnham S, Bourgeat P, Brown B, Ellis KA, Salvado O, et al. Amyloid beta deposition, neurodegeneration, and cognitive decline in sporadic Alzheimer's disease: a prospective cohort study. Lancet Neurol 2013; 12: 357–67.

Villemagne VL, Fodero-Tavoletti MT, Masters CL, Rowe CC. Tau imaging: early progress and future directions. Lancet Neurol 2015; 14: 114–24.

Wang DL, Zhang SY, Li LA, Liu X, Mei KR, Wang XQ. Structural insights into the assembly and activation of IL-1 beta with its receptors. Nat Immunol 2010a; 11: 905–U52.

Wang K, Li M, Hakonarson H. ANNOVAR: functional annotation of genetic variants from high-throughput sequencing data. Nucleic Acids Res 2010b; 38: e164.

Wang WF, Liao YC, Wu SL, Tsai FJ, Lee CC, Hua CS. Association of interleukin-I beta and receptor antagonist gene polymorphisms with late onset Alzheimer's disease in Taiwan Chinese. Eur J Neurol 2005; 12: 609–13.

Weiner MW, Aisen PS, Jack CR, Jr, Jagust WJ, Trojanowski JQ, Shaw L, et al. The Alzheimer's disease neuroimaging initiative: progress report and future plans. Alzheimers Dement 2010; 6: 202–11 e7.

Willer CJ, Li Y, Abecasis GR. METAL: fast and efficient meta-analysis of genomewide association scans. Bioinformatics 2010; 26: 2190–1.

Yang J, Lee SH, Goddard ME, Visscher PM. GCTA: a tool for genome-wide complex trait analysis. Am J Hum Genet 2011; 88: 76–82.

Yoder KK, Nho K, Risacher SL, Kim S, Shen L, Saykin AJ. Influence of TSPO genotype on 11C-PBR28 standardized uptake values. J Nucl Med 2013; 54: 1320–2.

Zhang B, Gaiteri C, Bodea LG, Wang Z, McElwee J, Podtelezhnikov AA, et al. Integrated systems approach identifies genetic nodes and networks in late-onset Alzheimer's disease. Cell 2013; 153: 707–20.

Zuk O, Schaffner SF, Samocha K, Do R, Hechter E, Kathiresan S, et al. Searching for missing heritability: designing rare variant association studies. Proc Natl Acad Sci USA 2014; 111: E455–64.